The Operation of Two Decarboxylases, Transamination, and Partitioning of C_4 Metabolic Processes between Mesophyll and Bundle Sheath Cells Allows Light Capture To Be Balanced for the Maize C_4 Pathway[1][W]

Chandra Bellasio* and Howard Griffiths

Physiological Ecology Group, Department of Plant Sciences, University of Cambridge, Cambridge CB2 3EA, United Kingdom

ORCID ID: 0000-0002-3865-7521 (C.B.).

The C_4 photosynthesis carbon-concentrating mechanism in maize (*Zea mays*) has two CO_2 delivery pathways to the bundle sheath (BS; via malate or aspartate), and rates of phosphoglyceric acid reduction, starch synthesis, and phospho*enol*pyruvate regeneration also vary between BS and mesophyll (M) cells. The theoretical partitioning of ATP supply between M and BS cells was derived for these metabolic activities from simulated profiles of light penetration across a leaf, with a potential 3-fold difference in the fraction of ATP produced in the BS relative to M (from 0.29 to 0.96). A steady-state metabolic model was tested using varying light quality to differentially stimulate M or BS photosystems. CO_2 uptake, ATP production rate (J_{ATP}; derived with a low oxygen/chlorophyll fluorescence method), and carbon isotope discrimination were measured on plants under a low light intensity, which is considered to affect C_4 operating efficiency. The light quality treatments did not change the empirical ATP cost of gross CO_2 assimilation (J_{ATP}/GA). Using the metabolic model, measured J_{ATP}/GA was compared with the predicted ATP demand as metabolic functions were varied between M and BS. Transamination and the two decarboxylase systems (NADP-malic enzyme and phospho*enol*pyruvate carboxykinase) were critical for matching ATP and reduced NADP demand in BS and M when light capture was varied under contrasting light qualities.

Interest in the C_4 pathway has been increased by the potential for enhancing crop productivity and maintaining yield stability in the face of global warming and population pressure (Friso et al., 2010; Zhu et al., 2010; Covshoff and Hibberd, 2012). Maize (*Zea mays*), a C_4 plant of the NADP-malic enzyme (ME) subtype, is a leading grain production cereal (www.fao.org). C_4 photosynthesis is a shared activity between mesophyll (M; abbreviations are listed in Table I) and bundle sheath (BS) cells, coupled to allow the operation of a biochemical carbon-concentrating mechanism (CCM). The CCM effectively minimizes photorespiration by increasing the CO_2 concentration in the bundle sheath (C_{BS}), where Rubisco is exclusively expressed. Since BS and M are connected by plasmodesmata, some CO_2 retrodiffuses. The refixation of that escaping CO_2 by the CCM increases the activity of the CCM and the total ATP demand ($ATP_{BS} + ATP_M$) for gross CO_2 assimilation (GA; $[ATP_{BS} + ATP_M]/GA$), from a theoretical minimum of five ATPs (Furbank et al., 1990).

Leakiness (Φ), the amount of CO_2 retrodiffusing relative to phospho*enol*pyruvate (PEP) carboxylation rate, is therefore a proxy for the coordination between the CCM and assimilatory activity (Henderson et al., 1992; Tazoe et al., 2008; Kromdijk et al., 2010; Ubierna et al., 2011; Bellasio and Griffiths, 2013).

Recently, the maize C_4 subgroup has been shown to be complicated by the presence of two BS decarboxylation enzyme systems (NADP-ME and phospho*enol*pyruvate carboxykinase [PEPCK]), presumably both acting as CO_2 delivery pathways (via malate [MAL] and Asp, respectively; Furumoto et al., 1999, 2000; Wingler et al., 1999; Eprintsev et al., 2011; Furbank, 2011; Pick et al., 2011). There is also an extensive overlap between BS and M functions, since both cell types can synthesize starch (Spilatro and Preiss, 1987; Kanai and Edwards, 1999) and reduce phosphoglyceric acid (PGA; Majeran and van Wijk, 2009; see the overall scheme in Fig. 1). Additionally, energetic partitioning can also vary between cell types, since the total ATP produced (J_{ATP}) per CO_2 fixed in GA (J_{ATP}/GA) may be produced in BS (mainly through cyclic electron flow [CEF] around PSI) or in M (mainly through linear electron flow [LEF]), depending on the light locally available in BS or M (Kramer and Evans, 2011; Yin and Struik, 2012). Furthermore, although all NADPH is produced in M, the only compartment operating linear electron transport and oxidizing water, some NADPH is exported to BS through MAL diffusion, to meet the reducing power demand therein ($NADPH_{BS}$). To capture the complex C_4 physiology, several models of C_4 photosynthesis have

Table I. *Variables and acronyms described in the text*

Abbreviation	Definition	Unit
A	Net assimilation	μmol m^{-2} s^{-1}
AB	Absorbed light	
AB BS/M	Partitioning of absorbed light	Dimensionless
ATP_{BS}	ATP demand in BS	μmol m^{-2} s^{-1}
ATP_M	ATP demand in M	μmol m^{-2} s^{-1}
BS	Bundle sheath	
C_{BS}	CO$_2$ concentration in BS	μmol mol^{-1}
CCM	Carbon-concentrating mechanism	
CEF	Cyclic electron flow	
DHAP	Dihydroxyacetone phosphate	
ETR	Electron transport rate	μmol m^{-2} s^{-1}
GA	Gross assimilation ($A + R_{LIGHT}$)	μmol m^{-2} s^{-1}
g_{BS}	Bundle sheath conductance to CO$_2$, calculated by fitting J_{MOD} to J_{ATP}	mol m^2 s^{-1}
IRGA	Infrared gas analyzer	
J_{ATP}	Total ATP production rate	μmol m^{-2} s^{-1}
J_{ATPBS}	ATP production rate in BS	μmol m^{-2} s^{-1}
J_{ATPM}	ATP production rate in M	μmol m^{-2} s^{-1}
J_{MOD}	Modeled ATP production rate	μmol m^{-2} s^{-1}
LEF	Linear electron flow	
LCP	Light compensation point	
M	Mesophyll	
MAL	Malate	
MDH	Malate dehydrogenase	
MDH_{BS}	Malate dehydrogenase reaction rate in BS	μmol m^{-2} s^{-1}
MDH_M	Malate dehydrogenase reaction rate in M	μmol m^{-2} s^{-1}
ME	Malic enzyme	
ME	Malic enzyme reaction rate	μmol m^{-2} s^{-1}
$NADPH_{BS}$	NADPH demand in BS	μmol m^{-2} s^{-1}
$NADPH_{TOT}$	Total NADPH demand	μmol m^{-2} s^{-1}
OAA	Oxaloacetic acid	
PAR	Photosynthetically active radiation	μE m^{-2} s^{-1}
PEP	Phospho*enol*pyruvate	
PEPCK	Phospho*enol*pyruvate carboxykinase	
$PEPCK$	PEPCK reaction rate	μmol m^{-2} s^{-1}
PGA	3-Phosphoglyceric acid	
PPDK	Pyruvate phosphate dikinase	
$PPDK$	PPDK reaction rate	μmol m^{-2} s^{-1}
PR	PGA reduction	
PR_{BS}	PR rate in BS	μmol m^{-2} s^{-1}
PR_M	PR rate in M	μmol m^{-2} s^{-1}
R_{BS}	Respiration in the light in BS	μmol m^{-2} s^{-1}
R_{LIGHT}	Respiration in the light	μmol m^{-2} s^{-1}
RPP	Reductive pentose phosphate	
RuBP	Ribulose-1,5-bisphosphate	
RuP	Ribulose-5-phosphate	
SS	Starch synthesis	
SS_{BS}	Starch synthesis rate in BS	μmol m^{-2} s^{-1}
SS_M	Starch synthesis rate in M	μmol m^{-2} s^{-1}
SS_{TOT}	Total starch synthesis rate	μmol m^{-2} s^{-1}
T	Transamination rate	μmol m^{-2} s^{-1}
V_C	Rubisco carboxylation rate	μmol m^{-2} s^{-1}
V_O	Rubisco oxygenation rate	μmol m^{-2} s^{-1}
V_P	PEP carboxylation rate	μmol m^{-2} s^{-1}
Y(II)	Yield of PSII	
Δ	^{13}C isotopic discrimination	‰
δ^{13}C	^{13}C isotopic composition relative to Pee Dee Belemnite	‰
Φ	Leakiness	Dimensionless

been developed (Berry and Farquhar, 1978; Laisk and Edwards, 2000, 2009; von Caemmerer, 2000). The earlier approaches were developed into the von Caemmerer (2000) C$_4$ model. In particular, the associated light-limited equations (referred to subsequently as the "C$_4$ model") are used to estimate the parameters needed to resolve the isotopic discrimination (Δ) model, widely employed to study Φ under low-light conditions (for review, see Ubierna et al., 2011). The C$_4$ model partitions J_{ATP} into two fractions: (1) the ATP consumed by PEP carboxylase, and (2) the ATP consumed by the C$_3$ activity (glyoxylate recycling, PGA reduction [PR], and ribulose 1,5-bisphosphate [RuBP] regeneration). These activities are located in M, BS, or both compartments (see the overall scheme in Fig. 1). However, the C$_4$ model simplifies the spatial compartmentalization between BS and M, and in this paper, we now develop the energetic implications of the differential contribution of M and BS to C$_4$ photosynthesis under different light regimes.

Because of these anatomical, metabolic, and energetic complexities, C$_4$ metabolism is highly sensitive to limiting light intensity (Bellasio and Griffiths, 2013) and, potentially, light quality (Evans et al., 2007). Light quality has a greater influence on C$_4$ photosynthesis than on C$_3$. Leaf pigments preferentially absorb the blue and red region of the spectra, and some wavelengths penetrate deeper into leaves. It was shown in C$_3$ leaves that exposure to different wavelengths results in characteristic light penetration profiles, which, translated into different gradients in PSII yield, rates of ATP production, and assimilation (A) within the leaf (Terashima et al., 2009). In C$_4$ leaves, because of the concentric anatomy, light reaches M cells before the deeper BS (Evans et al., 2007) and could alter the balance between light harvesting and energetic partitioning between BS and M.

In this paper, we model the likely profiles of light penetration for specific wavelengths associated with red, green, and blue light within a maize M and BS leaf cross section and calculate the impact on potential ATP production for each cell type. We calculate the proportion of absorbed light (AB) for each wavelength, expressed as AB BS/M, the fraction of photons absorbed in BS relative to the photons absorbed in M, from which we derive J_{ATPBS}/J_{ATPM}, the fraction of ATP produced in BS relative to the ATP produced in M. Second, we developed a steady-state metabolic model (Fig. 1; Table II), which augments the conventional C$_4$ model (von Caemmerer 2000), to capture the spatial separation between BS and M and partitions the ATP demand between BS and M cells in terms of PR, starch synthesis (SS), and PEP regeneration, so as to meet the ATP availability in each cell type (Evans et al., 2007). Third, photosynthetic characteristics (leaf-level ATP production rate, CO$_2$ assimilation, stomatal conductance, and Φ derived from online carbon isotope discrimination [Δ]) were measured under red, green, and blue light, and red, green, and blue light in combination (RGB), using a decreasing photon flux density (from 500 to 50 μE m^{-2} s^{-1}) to investigate the importance of metabolic plasticity under limiting light intensities.
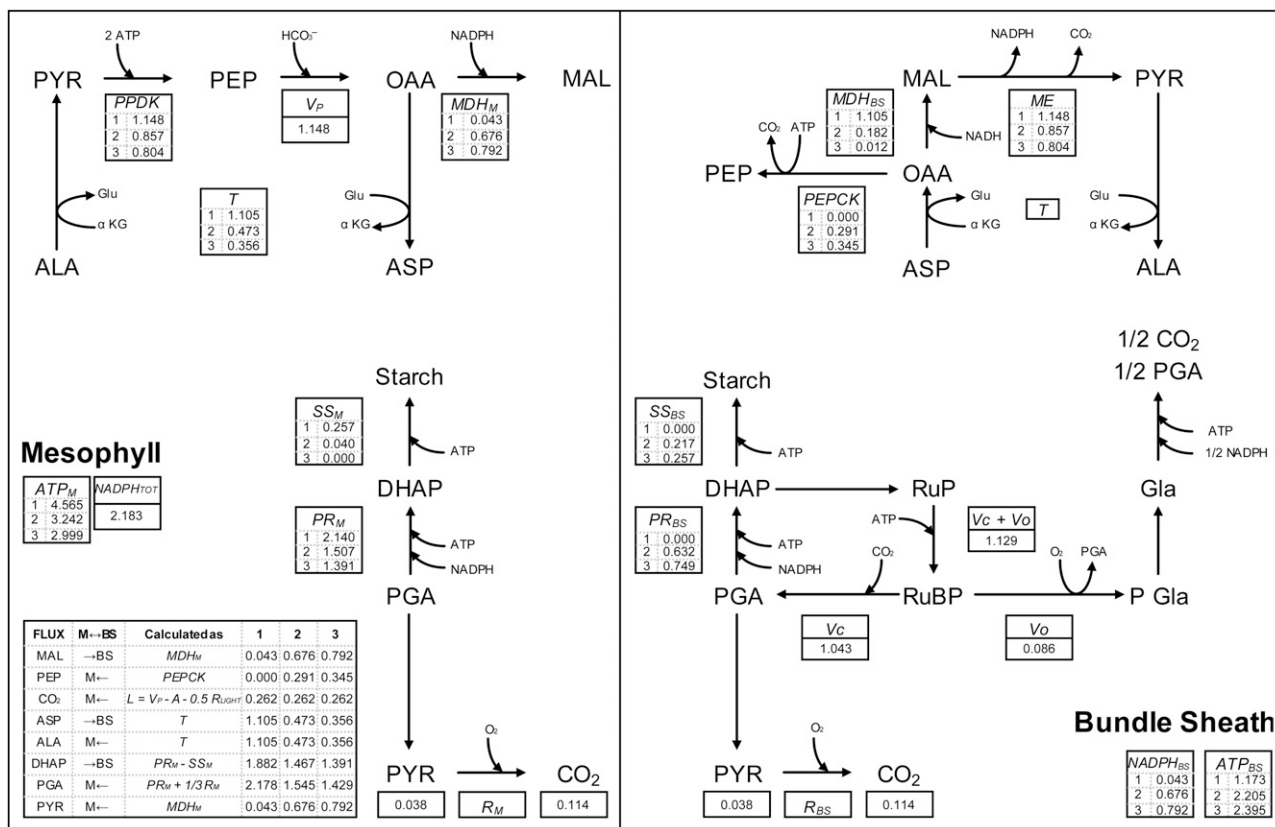
Figure 1. Metabolic model of C_4 assimilation, rates of reaction, and net fluxes between BS and M. The overall scheme reports the reactions of the CCM (Furbank, 2011), Rubisco carboxylation, the reactions of the RPP pathway, the synthesis of starch, respiration, and glyoxylate recycling reactions. The tables, with the corresponding enzyme names, show the actual reaction rates, expressed relative to GA (5.13 μmol m^{-2} s^{-1}), per unit of substrate transformed. Rates were estimated by parameterizing the model equations (Table II) with data measured under PAR = 125 μE m^{-2} s^{-1} ($A = 3.96$ μmol m^{-2} s^{-1}; $R_{LIGHT} = 1.17$ μmol m^{-2} s^{-1}; $J_{ATP} = 28.6$ μmol m^{-2} s^{-1}), the output of the C_4 model ($V_C = 5.35$ μmol m^{-2} s^{-1}; $V_P = 5.89$ μmol m^{-2} s^{-1}; $V_O = 0.44$ μmol m^{-2} s^{-1}), and the output of the Δ model ($\Phi = 0.23$) under three characteristic ratios of ATP partitionings. These were numbered 1, 2, and 3. Condition 1 corresponds to the lowest ATP available in BS (ATP partitioning similar to that under blue light; Fig. 4B), condition 2 corresponds to an intermediate ATP availability in BS (ATP partitioning equal to that under red light; Fig. 4B), and condition 3 corresponds to the highest ATP available in BS (ATP partitioning equal to that under green light; Fig. 4B). The inset shows net metabolite fluxes between M and BS in multiples of GA. The ATP demand in BS (ATP_{BS}) and M (ATP_M), the total NADPH demand ($NADPH_{TOT}$), and the $NADPH_{BS}$ were also calculated in the same three relevant conditions. PYR, Pyruvic acid.

For instance, AB BS/M and J_{ATPBS}/J_{ATPM} were both lower under the blue light (wavelength 460 nm), which is rapidly extinguished within the M leaf profile, than under white light, confirming that light quality perturbs C_4 energetics. In spite of this shift, when maize plants were exposed to different light qualities, there was no change in Φ, indicating that, at steady state, the coordination between CCM activity and Rubisco assimilation was retained (Ubierna et al., 2011; Sun et al., 2012). The modeled metabolic plasticity projected a window for ATP demand partitioning (ATP_{BS}/ATP_M), which matched the values for J_{ATPBS}/J_{ATPM} supply estimated under red, green, and blue light. We show that the plasticity of C_4 metabolism, and in particular the possibility of shifting between MAL and Asp as a primary carboxylase product, was of pivotal importance in

allowing the plasticity of ATP and NADPH demand. In conclusion, our study explains the extensive overlap between BS and M functions and the requirement for at least two decarboxylase systems in NADP-ME subtype plants such as maize, providing an explanation for empirical observations on the diversity of decarboxylase activities and PEP regeneration pathways (Rathnam, 1978; Chapman and Hatch, 1981; Wingler et al., 1999; Eprintsev et al., 2011; Furbank, 2011; Pick et al., 2011).

RESULTS

Metabolic Modeling of Partitioning between BS and M

The complexity of C_4 biochemistry (Furbank, 2011) was first integrated in a comprehensive steady-state

Table II. *Steady-state equations for the metabolic model of C$_4$ assimilation*

Processes described by Equations 4 to 10 can be calculated directly from the measured data for A, R_{LIGHT}, and the output of the von Caemmerer C$_4$ model (V_O, V_P, and V_C), while Equations 11 to 21 require prior allocation of SS, PR, and PEPCK. For simplicity, enzyme names in italics represent the enzyme reaction rate. For stoichiometric consistency, reaction rates are calculated as rates of substrate transformation.

Process	Symbol	Reaction Rate	Equation	Localization	Notes
Gross assimilation	GA		(4)		GA and R_{LIGHT} rates are expressed per CO$_2$.
RuP phosphorylation	–		(5)	BS	RuP phosphorylation supplies Rubisco carboxylating activity (V_C) together with oxygenating activity (V_O).
Total PR	PR_{TOT}		(6)	BS and M	This equation calculates the total rate of PR on the basis of the PGA produced by Rubisco carboxylation ($2V_C$), Rubisco oxygenation (V_O), and glyoxylate recycling ($0.5V_O$) and considers the PGA consumed by respiration; $1/3$ is the stoichiometric conversion between respiration (expressed per CO$_2$) and PR (expressed per triose).
Total NADPH demand	$NADPH_{TOT}$		(7)	BS and M	PR consumes one NADPH per PGA; the total rate of PR is PR_{TOT} (see note to Eq. 6); in glyoxylate regeneration (per glyoxylate), 0.5 NADH is produced by Gly decarboxylase, 0.5 NADH is consumed by hydroxypyruvate reductase, and one ferredoxin (equivalent to 0.5 NADPH) is consumed by Gln synthetase; in total, 0.5 NADPH is consumed per glyoxylate (equivalent to V_O rate; Supplemental Table S1; Yoshimura et al., 2004).
DHAP entering RPP	–		(8)	BS	The DHAP entering the RPP pathway corresponds to the total PR rate minus the DHAP used for starch synthesis, which in this work is expressed per triose.
Total SS	SS_{TOT}		(9)	BS and M	In this model, assimilation is entirely converted to starch; this assumption does not influence energetics, as starch synthesis has the same ATP demand as phloem-loaded Suc; in Equation 9, 1/3 converts the stoichiometry of A (expressed per CO$_2$) to the stoichiometry of SS (expressed per triose).
Total PEP regeneration	–		(10)	BS and M	PEP regeneration rate equals PEP consumption rate V_P at steady state; PEP can be regenerated either by PPDK (mainly in M but active also in BS) or by PEPCK in BS; in this study, PPDK activity was assumed to be zero in BS.
Total ATP demand	ATP_{BS} + ATP_M		(11)	BS and M	Equation 11 calculates the total ATP demand as the sum of ATP demand for PR (one ATP per PGA, corresponding to PR), RuBP regeneration (one ATP per RuP, corresponding to V_C + V_O), glyoxylate recycling (one ATP per glyoxylate, corresponding to V_O), starch synthesis (0.5 ATP per triose, corresponding to SS), and PEP regeneration (one ATP per PEPCK catalytic event or two ATP per PPDK catalytic event); compared with the original formulation of the C$_4$ model, Equation 11 separates the ATP demand for PEPCK and PPDK, includes the ATP demand for SS, and considers the PGA utilized by respiration, which does not need to be reduced (see Eq. 6).
ATP demand in BS	ATP_{BS}		(12)	BS	The ATP demand in BS is brought about by PR (at the rate of PR_{BS}), RuBP regeneration (at the rate of V_C + V_O), glyoxylate recycling (at the rate of V_O), starch synthesis (0.5 ATP per triose), and PEPCK activity (one ATP per OAA; see note to Eq. 11).
ATP demand in M	ATP_M		(13)	M	The ATP demand in M is brought about by PR (at the rate of PR_M), SS, and PPDK (two ATPs per pyruvic acid; see note to Eq. 11).
NADPH demand in BS	$NADPH_{BS}$		(14)	BS	The NADPH demand in BS is brought about by PR (one NADPH per PGA) and glyoxylate recycling, which consumes 0.5 NADPH per glyoxylate (corresponding to V_O; see Supplemental Table S2).
NADPH supply to BS	–		(15)	BS	All NADPH available in BS is produced in M and exported through the MAL shuttle because we have assumed that no linear electron transport (i.e. water oxidation) occurred in BS; for this reason, the NADPH supply to BS corresponds to the NADPH consumed to reduce OAA to MAL in M, the process responsible for NADPH export, and not to the rate of MAL decarboxylation in BS, which depends on T, PEPCK, and MDH_{BS} (Eq. 19).
MDH activity in M	MDH_M	MDH_M	(16)	M	MDH activity supplies the NADPH demand in BS; Equation 16 was derived from Equations 14 and 15.
Transamination	T		(17)	BS and M	Equation 17 expresses that, at steady state, all OAA is either transaminated or reduced; since T bypasses the MDH_M reaction, which is the reaction responsible for NADPH export to BS (see note to Eq. 15), T has the function of balancing NADPH supply and demand, which becomes apparent when Equations 15 and 17 are combined.

(*Table continues on following page.*)

Table II. (*Continued from previous page.*)

Process	Symbol	Reaction Rate	Equation	Localization	Notes
MDH	MDH_{BS}	$T - PEPCK$	(18)	BS	MDH is assumed to operate a fast conversion at equilibrium; therefore, it is passively regulated by the substrate availability: the OAA that is not used by PEPCK is reduced to MAL by MDH; MDH may use NADH, since no NADPH-dependent reduction of OAA has been observed in maize (Kanai and Edwards, 1999) and it is likely mitochondrial (Rathnam, 1978; Chapman and Hatch, 1981); the NADH regeneration may be carried out by chloroplastic ME, which is reported to react both with NADP and NAD (Chapman and Hatch, 1981); however, the process may be more complicated (Eprintsev et al., 2011, and refs. therein); note that in this study, we assumed that cells are decompartmentalized while PEPCK rate was manipulated to increase between zero and a maximum rate in response to ATP availability (see "Minimum and Maximum BS Allocation" for details).
ME	ME	$MDH_M + MDH_{BS}$	19	BS	Equation 19 expresses that the rate of MAL oxidation by ME corresponds to the rate of MAL produced by MDH activity in M plus the rate of MAL produced by MDH activity in BS.
PPDK	$PPDK$	$V_P - PEPCK$	20	M	The PEP regenerated by PEPCK in BS diffuses to M and reduces the requirement of PEP regenerated by PPDK in M.
PR in M	PR_M	$PR_{TOT} - PR_{BS}$	21	M	PR is a shared process between BS and M.

model (Fig. 1), with key processes described by rate equations (Fig. 1, box; Table II) and associated ATP demand (Eqs. 11–13 in Table II). This model captures the spatial separation between BS and M, the different pathways of the CCM (through Asp and MAL), the different carboxylating enzymes, and the process of SS, as a means to develop the traditional C$_4$ model (von Caemmerer 2000). The metabolic model (Fig. 1) was generated on the assumption that ATP does not freely diffuse between BS and M and any light-induced J_{ATPBS}/J_{ATPM} fluctuations have to be countered by changing the partitioning of ATP demand (for a list of abbreviations, see Table I). Figure 1 depicts the reactions that are localized in BS, in M, or in both compartments. Ribulose-5-phosphate (RuP) phosphorylation is uniquely localized in BS to supply RuBP directly in proximity to Rubisco and facilitate the substrate saturation of the enzyme. Glyoxylate recycling is also a BS-exclusive reaction (Fig. 1; Yoshimura et al., 2004). This feature contributes to the CCM (the so-called C$_2$ cycle), and in an evolutionary perspective, it was acquired at an early stage (Sage et al., 2012; Schulze et al., 2013). PEP regeneration through PEPCK is located uniquely in BS (Wingler et al., 1999), while PEP regeneration through pyruvate phosphate dikinase (PPDK) is located primarily in M (Fig. 1; Friso et al., 2010; Majeran et al., 2010), and any PPDK activity in BS is generally neglected (von Caemmerer, 2000; see "Discussion"). PR, respiration, and SS are processes located both in BS and M (Spilatro and Preiss, 1987; Kanai and Edwards, 1999; Majeran and van Wijk, 2009; Friso et al., 2010).

These processes are described in detail below, after an initial comparison of modeled light profiles and measured photosynthetic characteristics under red, green, and blue wavelengths, to give a quantitative description of the biochemical mechanisms underpinning acclimation, fluxes and reaction rates, the dynamics of Φ, and the effects on the total and relative ATP demand for assimilation.

Effect of Light Quality on ATP Production in BS and M

To study the influence of light quality on J_{ATPBS}/J_{ATPM}, we first modeled C$_4$ anatomy (Fig. 2, left). Light penetration was modeled in two characteristic profiles using the absorption-scattering theory (Fig. 2, right). Profiles were calibrated with leaf transmittance and reflectance at different wavelengths. Blue light was strongly absorbed (steep profile), green light was weakly absorbed (gradual profile), while red light had an intermediate profile of light penetration. These three profiles were integrated to estimate the contribution of absorbed light within adaxial + abaxial M, interveinal M, and BS (Fig. 2) and calculated the partitioning of AB BS/M under five relevant conditions (Table III). AB BS/M was used in turn to estimate J_{ATPBS}/J_{ATPM} (Table III) under the assumption that photochemical yield did not vary through the leaf profile (see "Materials and Methods"). At 400 nm, AB BS/M was lowest, representing J_{ATPBS}/
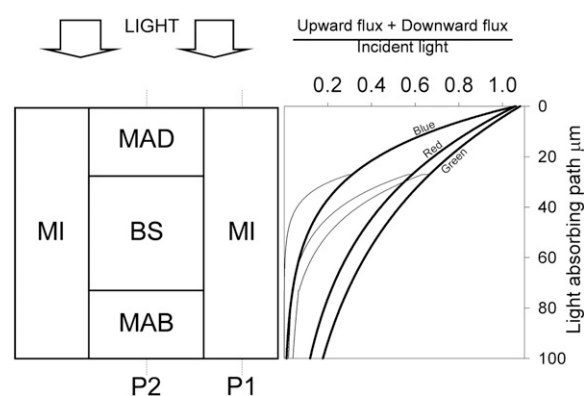
Figure 2. Light penetration in a maize leaf. At left is the modeled maize anatomy. A square BS is surrounded by three portions of M: interveinal M (MI), adaxial M (MAD), and abaxial M (MAB). Epidermis was approximated as a flat reflecting surface. Light penetration was studied through profiles P1 and P2. At right are P1 light profiles (thick lines) and P2 light profiles (thin lines) calculated with the Kubelka-Munk (absorption + scattering) theory and calibrated with spectroscopic data (Table III). Radiation is expressed as the sum of downward + upward photon flux, as a fraction of incident photon flux (dimensionless), and plotted against the depth in the absorbing path of the leaf.

J_{ATPM} of 0.29; at 540 nm, AB BS/M was highest together with J_{ATPBS}/J_{ATPM} (0.96). Under blue light, J_{ATPBS}/J_{ATPM} was close to the lowest value (0.31), increasing under red light (0.68), natural white light (0.76), and green light (0.80). These values were derived independently of light intensity, so they can be considered to represent the actual ATP availability in BS and M under a wide range of light intensities. Since ATP does not diffuse between BS and M and has a relatively small pool, at steady state, J_{ATPBS}/J_{ATPM} can be directly compared with ATP_{BS}/ATP_M. For this comparison, the values for J_{ATPBS}/J_{ATPM} under blue, red, white, and green light were used subsequently to plot Figure 4B below. The model predicts that light quality will unbalance the partitioning of ATP production. A comprehensive ecophysiological investigation was undertaken to study how assimilation and conversion efficiency would be affected.

Effect of Light Quality on Assimilatory Traits

Figure 3 shows the responses of maize to different light qualities (red, green, blue, or RGB) measured under decreasing irradiance. Net A, measured through gas exchange (Fig. 3A), and J_{ATP}, measured with the low oxygen-electron transport rate (ETR) method using a saturating light pulse (Fig. 3B), were significantly higher under red light and decreased under RGB, green, and blue. Light quality had no significant effect on stomatal conductance (Supplemental Fig. S1A), but Ci/Ca (for substomatal CO$_2$ concentration/cuvette CO$_2$ concentration) was lower under red light (Supplemental Fig. S1B) as a consequence of the higher A. The C_{BS}, estimated by fitting a C$_4$ photosynthesis model to J_{ATP}, was higher

Table III. *Energy partitioning between BS and M at different wavelengths*

Measured leaf reflectance and transmittance (Woolley, 1971) was used to parameterize the optical model (Fig. 2) to calculate the likely profiles of light penetration at different wavelengths. AB BS/M was calculated integrating such light absorption profiles (Fig. 2, right) over the corresponding BS and M areas (Fig. 2 left) and used to calculate J_{ATPBS}/J_{ATPM} (Eq. 3).

Wavelength	Description	Reflectance	Transmittance	AB BS/M	J_{ATPBS}/J_{ATPM}
nm			%		
400	Lowest AB BS/M	4	0.1	0.15	0.29
460	Blue light-emitting diode used	5	1	0.16	0.31
635	Red light-emitting diode used	6	7	0.34	0.68
400–700	Natural white light	8	9	0.38	0.76
522	Green light-emitting diode used	8	11	0.40	0.80
540	Highest AB BS/M	13	23	0.48	0.96

under red and green light (Supplemental Fig. S1C) because of the higher *A*. The light compensation point (LCP), BS conductance (g_{BS}), and respiration in the light (R_{LIGHT}) were not significantly influenced by light quality (Table IV).

With the precise estimate of R_{LIGHT} and J_{ATP}, we calculated J_{ATP}/GA, which represents the experimentally determined ATP cost for gross assimilation. J_{ATP}/GA was not influenced by light intensity but varied between light qualities from 5.73 to 5.37 under blue, red, RGB, and green light. J_{ATP}/GA was then used in Figure 4B, plotted against the J_{ATPBS}/J_{ATPM} found above. The relatively minor increase in J_{ATP}/GA (approximately 0.4 ATP per CO_2) observed experimentally contrasts with the metabolic disruption theoretically predicted under these conditions (Evans et al., 2007). Our data were supported by real-time Δ (Fig. 3C) and Φ (Fig. 3D), which were not influenced by light quality, showing that the plant coped with a 2.5× shift in J_{ATPBS}/J_{ATPM} without any imbalance in the coordination of CCM activity and assimilation. Obtaining Φ data under such low light intensities represents a technical challenge, and the experimental protocol was carefully optimized for low light intensity (Bellasio and Griffiths, 2013). Data obtained under low light are subject to a potential error magnification due to the small difference in CO_2 concentration between the air entering and leaving the cuvette (Supplemental Fig. S2; Evans et al., 1986), as clearly shown by the large error bars in Figure 3D, and therefore should be interpreted with care. Φ, J_{ATP}/GA, and the window of J_{ATPBS}/J_{ATPM} formed the basis of a metabolic model used to describe these biochemical responses.

Influence of BS Activity on Assimilatory Metabolism and ATP Demand (Total and Relative)

The comprehensive metabolic model (Fig. 1) was developed to describe the biochemical reactions directly and indirectly involved in C_4 assimilation by rate equations (Table II). The proportions of three assimilatory ATP-consuming processes (SS, PR, and PEPCK) were manipulated to increase within BS (allocated; Fig. 4A). These processes overlap between BS and M and could be allocated to BS without influencing the overall assimilation rate. By means of this progressive allocation, we predicted the following: (1) the minimum and maximum ATP_{BS}/ATP_M (Eqs. 12 and 13 in Table II); (2) the reaction rates and metabolite fluxes at a given ATP_{BS}/ATP_M, including the rate of PEPCK and PPDK, the relative CO_2 flux through Asp and MAL, and the partitioning of PR between BS and M; and (3) the dynamics of $(ATP_{BS} + ATP_M)/GA$ at variable ATP_{BS}/ATP_M.

When the BS allocation rate of PR, PEPCK, and SS was zero (referred as condition 1; no. 1 in Figs. 1 and 4B), the predicted ATP_{BS}/ATP_M was lowest (0.27). This value was comparable to J_{ATPBS}/J_{ATPM} resolved from the optical model under blue wavelengths (400 and 460 nm; Table III), showing that metabolism could reduce ATP demand to match even the lowest ATP supply in BS. In this condition, the ATP demand in BS was brought about by RuP phosphorylation and glyoxylate recycling, two processes that are known to be exclusive to BS. The predicted $(ATP_{BS} + ATP_M)/GA$ was 5.74 (Fig. 4B, dashed line), in agreement with J_{ATP}/GA measured under blue light (5.73; Fig. 4B, blue square). Since photosynthetic PGA production is exclusive to BS (from Rubisco carboxylase or oxygenase activity, and glyoxylate recycling), when there is no ATP available for PR (e.g. in condition 1), the PGA diffuses to M and is reduced to dihydroxyacetone phosphate (DHAP) therein. The predicted $NADPH_{BS}$, therefore, was the lowest (Eq. 14 in Table II; Fig. 4A, dotted line), corresponding to the NADPH demand for glyoxylate recycling in BS. DHAP supplies SS in M and diffuses back to BS where it is used to regenerate RuBP. The activity of malate dehydrogenase (MDH) in M (MDH_M), a process responsible for exporting NADPH, was reduced by diverting the substrate oxaloacetate (OAA) to transamination to Asp. Hence, in condition 1, MDH_M had the lowest activity (Fig. 1; Eq. 16 in Table II), while transamination had the highest rate (Figs. 1 and 4A, dashed line; Eq. 17 in Table II). Once Asp diffused to BS, it underwent a futile reduction-oxidative decarboxylation that resulted in net CO_2 flux without a conjoint NADPH translocation (Fig. 1).

When PR and SS were progressively allocated in BS, the predicted ATP_{BS}/ATP_M (Figs. 1 and 4) progressively increased. The activation of PEPCK in BS not only contributed to the predicted increasing ATP demand in BS but also lowered the predicted ATP cost of
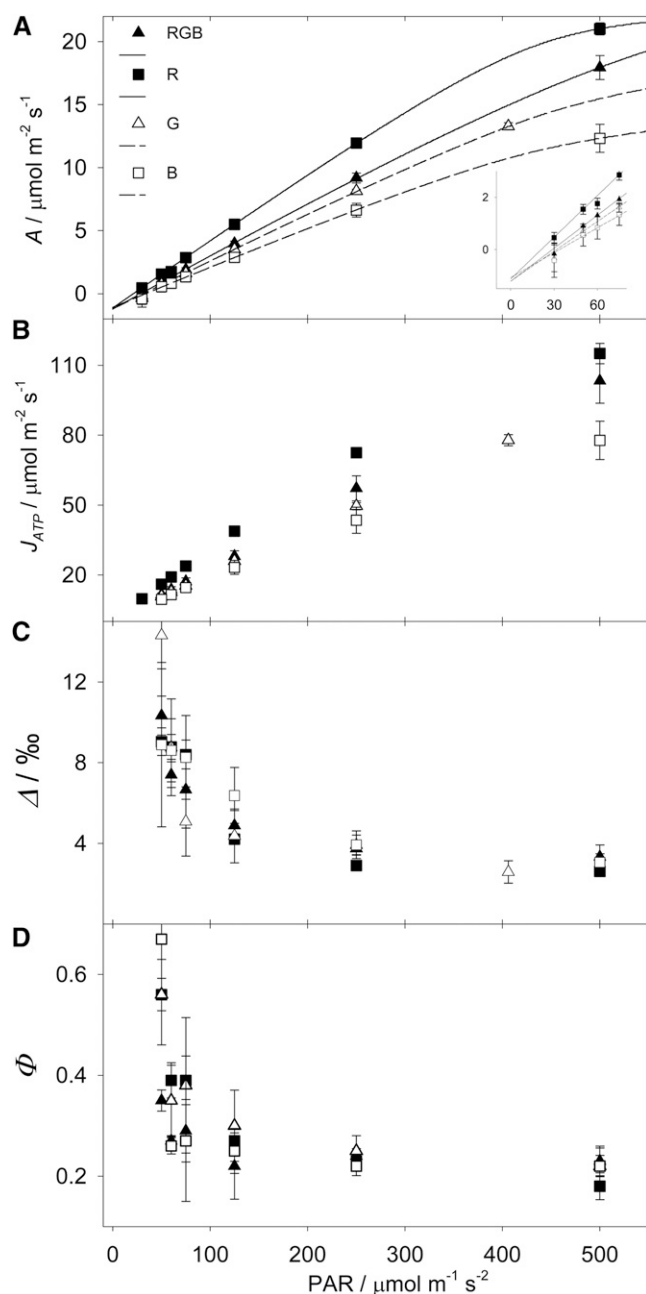
Figure 3. Maize responses to decreasing light intensity under different light qualities. A, Net *A*. The curves were fitted in order to calculate the light compensation point (Table IV). The inset shows a magnification. B, J_{ATP}, measured with the low oxygen-ETR method. C, Online Δ during photosynthesis. D, Φ resolved from Δ. Error bars represent SE; $n = 4$. B, Blue light; G, green light; R, red light.

assimilation $(ATP_{BS} + ATP_M)/GA$, because PEPCK regenerates PEP with half the ATP demand of PPDK. Condition 2 (no. 2 in Figs. 1 and 4) represents a state where ATP_{BS}/ATP_M equals J_{ATPBS}/J_{ATPM} resolved from the optical model under red light (0.68; Table III). The predicted $(ATP_{BS} + ATP_M)/GA$ (5.45; Fig. 4B, dashed line) agreed with J_{ATP}/GA measured under red light (5.47; Fig. 4B, red square).

When the projected allocation of PR, PEPCK, and SS to BS was highest (referred to as condition 3; no. 3 in Figs. 1 and 4A), the predicted ATP_{BS}/ATP_M was 0.8. This partitioning equals J_{ATPBS}/J_{ATPM} estimated by the optical model under green light and is similar to J_{ATPBS}/J_{ATPM} estimated under natural white light (0.76; Table III). Because PEPCK was activated at the highest rate, only 70% of PEP was regenerated through PPDK and $(ATP_{BS} + ATP_M)/GA$ was lowest (5.39; Fig. 4B, dashed line), predicting well J_{ATP}/GA values measured under RGB (5.38; Fig. 4B, RGB square) and green light (5.37; Fig. 4B, green square). In condition 3, PR in BS was highest, determining the highest $NADPH_{BS}$ (Figs. 1 and 4A, dotted line; Eq. 14 in Table II) and the highest MDH_M activity (Fig. 1; Eq. 16 in Table II). Because most of the OAA produced by PEP carboxylase was reduced by MDH_M, the transamination rate was lowest, just enough to supply PEPCK activity in BS.

Estimate of Actual Reaction and Diffusion Rates

Since all C$_4$ reactions were described by rate equations (Table II), we could estimate actual reaction rates. Although the predictions shown so far (including the optical part) are largely independent of light intensity, in this step, rates had to be calculated at a specific light intensity. However, in order to compare these values in a wider range of light intensities, rates were expressed as relative to *GA*. This also had the advantage of avoiding any computational distortion caused by respiration in the vicinity of the light compensation point. The irradiance of 125 μE m^{-2} s^{-1}, characteristic of illumination in the shade, was chosen because ongoing studies on low light and light quality are relevant to the physiology of shading (see "Discussion"). Furthermore, since low light provides a means to directly manipulate C$_4$ metabolism, a great deal of comparable work has been undertaken both in this laboratory (Kromdijk et al., 2008, 2010; Bellasio and Griffiths, 2013) and by other investigators (Ubierna et al., 2011, 2013) under low irradiances. Reaction rates, shown in the boxes within Figure 1, were obtained by parameterizing the model with the data obtained during the experiment and with the output of the C$_4$ model (all equations are reported in Supplemental Table S1; see also Bellasio and Griffiths [2013] and refs. therein). Rates were calculated for the three relevant conditions mentioned above (i.e. condition 1 corresponds to the lowest ATP demand in BS, condition 2 corresponds to an intermediate ATP demand [matching ATP supply under red light], and condition 3 correspond to the highest ATP demand in BS [matching ATP supply under green light]). Conditions 1, 2, and 3 are numbered 1, 2, and 3 in Figures 1 and 4.

DISCUSSION

The implications of the metabolic model for partitioning ATP demand are first considered in terms of previous studies of C$_4$ decarboxylases in NADP-ME

Table IV. *Physiological responses of maize plants to different light qualities*

The LCP was determined by fitting light curves with dedicated software; R_{LIGHT} was determined by linear regression of A against PAR $\times$ Y(II)/3; g_{BS} was determined by fitting a modeled J_{MOD} to the measured J_{ATP} (Fig. 3). Differences were not significant for $P < 0.05$. Values shown are means $\pm$ SE; $n = 4$.

Parameter	Unit	Mean	RGB	Red	Green	Blue
LCP	μE m^{-2} s^{-1}	29.04	28.05 $\pm$ 1.8	21.24 $\pm$ 3.1	33.10 $\pm$ 4.1	33.75 $\pm$ 5.7
R_{LIGHT}	μmol oxygen m^{-2} s^{-1}	1.169	1.202 $\pm$ 0.090	1.231 $\pm$ 0.11	1.148 $\pm$ 0.11	1.095 $\pm$ 0.12
g_{BS}	mol m^{-2} s^{-1}	0.00104	0.00127 $\pm$ 3.1 $\times$ 10^{-4}	0.00117 $\pm$ 3.1 $\times$ 10^{-4}	0.00075 $\pm$ 3.1 $\times$ 10^{-4}	0.00247 $\pm$ 3.1 $\times$ 10^{-4}

systems. The resultant ATP partitioning and metabolic plasticity provided by these processes are then considered in terms of overall C$_4$ energetic limitations (Evans et al., 2007). Finally, we consider the implications for multiple decarboxylase origins and function in terms of C$_4$ pathway evolution as well as light use and energy partitioning within a C$_4$ crop canopy.

Modeling ATP Demand: Decarboxylase Diversity in C$_4$ Systems

Recent developments in C$_4$ research have highlighted the complexity of C$_4$ metabolism in terms of extensive overlapping of BS and M functions (Friso et al., 2010; Majeran et al., 2010), the presence of transamination and two distinct decarboxylating pathways (Meister et al., 1996; Wingler et al., 1999; Pick et al., 2011), and plasticity in MAL metabolism (Eprintsev et al., 2011, and refs. therein). Although an involvement in balancing the energetic capacity in response to environmental conditions has been proposed (Furbank, 2011), empirical evidence and an associated metabolic model were needed to validate this suggestion. In this study, we tested the capability of metabolism to respond to different ATP allocations between BS and M by means of a comprehensive metabolic model. To overcome uncertainties in the causal relationship between ATP availability and enzyme kinetics, we deduced the highest and lowest possible BS reaction rates from physiological considerations and studied how the predicted ATP_{BS}/ATP_M would vary in response to incremental activation. We found that ATP_{BS}/ATP_M could vary between 0.27 to 0.80 if SS, PR, and PEP regeneration were freely allocated between BS and M. In particular, the rate of PEP regeneration in BS was modulated by manipulating the engagement of PEPCK. The availability of PEPCK in BS and the possibility to engage PEPCK at a variable rate had a twofold importance. Firstly, it expanded the window of ATP_{BS}/ATP_M to match the predicted window of J_{ATPBS}/J_{ATPM}. Secondly, it allowed to closely predict the decreasing ATP cost of GA at increasing J_{ATPBS}/J_{ATPM}, observed experimentally. In other words, metabolism could take advantage of the increased ATP availability in BS under penetrating light quality by activating PEPCK, which regenerates PEP with half the ATP cost of PPDK in M. In addition, we suggest that higher ATP consumption in BS than the predicted maximum could result from the transient activation of PPDK in BS (Aoyagi and Nakamoto, 1985; Friso et al.,

2010) or in a long-term response from the de novo synthesis of PR enzymes. This shows the importance of the presence of PPDK in BS and the possibility of metabolism to regulate the maximum BS rate of PR in response to contrasting environmental conditions. These processes could take advantage of the increased ATP availability in BS under 540-nm green light (Table III) or under high irradiances when ATP production in M is reduced (because of PSII yield quenching; Supplemental Fig. S3).

The extensive overlap between BS and M functions was important for preserving the overall assimilation rate, and for any process activated in BS, a complementary decrease in M could rebalance overall metabolism so that the total rate of assimilation and ATP demand remained constant in spite of contrasting BS/M engagement. In addition, we showed the importance of transamination rate (T) in balancing the reducing power needs in BS. When the ATP availability in BS was low (e.g. condition 1), PR in BS was downregulated; therefore, there was a lower NADPH demand in BS (Fig. 4A, dotted line). Under these conditions, CO$_2$ was delivered to BS through Asp, a pathway that bypasses MAL reduction in M and, hence, NADPH export to BS. This shift between Asp- and MAL-mediated CCM indicates the importance of maintaining both pathways in NADP-ME subtype C$_4$ plants. The predicted T varied in response to environmental conditions from a minimum PEP carboxylation rate (V_P) of 0.35 to the entirety of the CO$_2$ delivered to BS, in line with the observation that Asp can support physiological rates of photosynthesis (Rathnam, 1978; Chapman and Hatch, 1981; Meister et al., 1996; Pick et al., 2011). Under white light, the model predicted a 33% T/V_P, which is in line with radiolabeling and biochemical observations (Downton, 1970; Hatch, 1971; Chapman and Hatch, 1981). These predictions are not influenced by whether transamination is mediated by Glu aminotransferases (Fig. 1) or by the more recently documented Asp aminotransferases (Pick et al., 2011), because, in the model, transamination is simply assumed to be a fast, passively regulated process at equilibrium. In addition, having two independent pathways of CO$_2$ delivery (through MAL and Asp) decreases the MAL concentration gradient required to sustain a physiological assimilation rate (Pick et al., 2011).

Although a mechanistic explanation goes beyond the scope of this study, it is worth noting that the fine-tuning
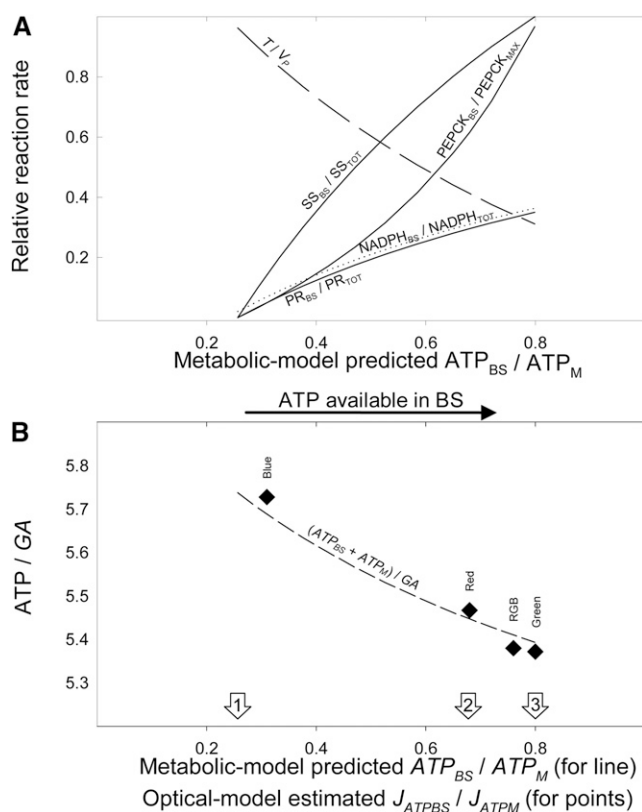
Figure 4. Partitioning of metabolic activities in BS cells and associated shifts in ATP and NADPH demand. A, The output of the metabolic model, shown as a function of increasing theoretical ATP_{BS}/ATP_M: the increasing contribution of BS (solid lines) to the total PR (relative to the total), SS (relative to the total), and PEPCK (relative to the highest rate); the predicted NADPH demand in BS (relative to the total [$NADPH_{BS}/NADPH_{TOT}$]; dotted line); and the predicted T (relative to V_P [T/V_P]; dashed line). B, The output of the metabolic model is compared with the empirical data. Model output is shown by the dashed line: the predicted $(ATP_{BS} + ATP_M)/GA$ is plotted as a function of the predicted ATP_{BS}/ATP_M. Empirical data are shown as diamonds: the measured J_{ATP}/GA, under blue, red, RGB, and green light (Table I), is plotted against the estimated ATP production partitioning J_{ATPBS}/J_{ATPM} at 460 nm, 635 nm, white light, and 522 nm (estimated through the optical model; Table III). The lowest ATP_{BS}/ATP_M was named condition 1 (left arrow), the partitioning corresponding to red light was named condition 2 (middle arrow), and the highest ATP_{BS}/ATP_M was named condition 3 (right arrow).

between contrasting scenarios may be relatively straightforward at the metabolic level. In fact, both the CCM and the reductive pentose phosphate (RPP) pathways share diffusible metabolites between BS and M cells and are mediated by fast reactions, which, in physiological conditions, are close to the thermodynamic equilibrium (e.g. transamination reactions or sugar phosphate conversions). The regulation of the fluxes, therefore, may be regulated in just a few key steps, for instance, at the level of PR or MAL decarboxylation. These have long been known to be regulated by the stromal pH, by feedback from metabolite pools, and by feed forward from light reactions

(Johnson and Hatch, 1970; Drincovich and Andreo, 1994; Detarsio et al., 2003; Murmu et al., 2003; Trost et al., 2006; Eprintsev et al., 2011). The adjustment of the other reaction and diffusion rates may then follow passively, mediated by the feedback provided by changing relative metabolite concentrations in one or the other compartment.

Modeling ATP Supply as a Function of Light Quality

Previously, fluorescence microimaging had shown that, because of the characteristic C$_4$ concentric leaf anatomy, strongly absorbed blue wavelengths would result in preferential absorption in M cells as compared with wavelengths of light that could penetrate deeper into the leaf profile (Evans et al., 2007). However, difficulties in the interpretation of fluorescence imaging, which are dependent on the different fluorescence yields of PSI-rich BS and PSII-rich M, have prevented investigators from predicting the relative light harvesting in BS and M (Evans et al., 2007). To overcome these difficulties, we characterized the profiles of light penetration in a maize leaf by means of an absorption-scattering model, which represents, to our knowledge, a first attempt to calculate the extent of light absorption imbalance caused by light quality. Because both BS and M produce ATP in light reactions, light harvesting imbalances would alter ATP partitioning. These ATP production imbalances were estimated using the relative stoichiometry of the electron transport operating in BS and M. The effect was very different from the response to changing light intensity; in fact, light quality only marginally influenced the total ATP available at the leaf level but resulted in a 3-fold difference in the fraction of ATP produced in the BS, from 0.29 to 0.96 (Table III). These imbalances are potentially independent of the light intensity; however, photochemical yield (i.e. quenching) was assumed to be independent of the position within the leaf (see description of Eq. 3 below), an assumption that may not hold under high light intensity. Regulation of photosystem yield through the leaf profile (Terashima et al., 2009) might also occur under changing light quality. Differential quenching would represent an additional point of plasticity in response to changing light quality, which would have the effect of narrowing the window of possible ATP_{BS}/ATP_M. Since we were interested in biochemical plasticity in response to ATP imbalance rather than in detailing the mechanics of electron transport processes, we did not include the possible plasticity at the thylakoid level and, hence, maximized the operating range of possible ATP_{BS}/ATP_M variation.

This spatial partitioning of ATP production (J_{ATPBS}/J_{ATPM}) is different from the functional partitioning of ATP consumption of the C$_4$ model (von Caemmerer, 2000; Ubierna et al., 2011; Bellasio and Griffiths, 2013) and from the theoretical ATP_{BS}/ATP_M of the metabolic model presented here. In the C$_4$ model, the J_{ATP} is simply assumed to be produced by an undivided electron

transport chain (Yin and Struik, 2012) and then partitioned to PEP regeneration activity or C_3 activity by a parameter known as x (Supplemental Table S1). This operation does not involve spatial separations between BS and M. In this study, we followed this conventional approach, which has been widely validated, and then captured the partitioning between BS and M with the equations of the metabolic model (Table II). On the basis of this division of work, we calculated the theoretical ATP_{BS}/ATP_M. Values for ATP_{BS}/ATP_M, therefore, were derived independently from J_{ATPBS}/J_{ATPM} (J_{ATPBS}/J_{ATPM} was not used in model parameterization). These independently derived J_{ATPBS}/J_{ATPM} and ATP_{BS}/ATP_M values were compared in Figure 4.

Implications for Electron Transport Processes

To allow these ATP partitioning rearrangements, there must be a high degree of flexibility at the electron transport chain level. In fact, although LEF activity in BS is often neglected (because of negligible expression of the oxygen-evolving complex [Majeran and van Wijk, 2009; Friso et al., 2010] and nonappreciable oxygen-evolving activity [Meierhoff and Westhoff, 1993]), evidence that appreciable linear flow can be supported by stromal reductants such as glutathione and ascorbate has been presented (Walker and Izawa, 1979; Ivanov et al., 2001, 2005, 2007). These reductants are likely to be produced from NADPH, supplied by MAL imported from M (Kanai and Edwards, 1999; Laisk and Edwards, 2000). These processes couple reductant pools at the thylakoid and stromal levels and are likely to function as plasticity mechanisms, playing a pivotal role in acclimation to changing light conditions.

Most of the LEF activity is localized in M chloroplasts, which evolve oxygen and supply all reducing power requirements. For this reason, many reactions requiring NADPH (such as nitrogen reduction) are localized in M to benefit from NADPH availability (Majeran et al., 2005). Even if M chloroplasts are specialized in NADPH production, the ratio of ATP to NADPH demand is highly sensitive to BS/M assimilation partitioning (Fig. 1). Meeting this variable requirement will involve differential engagement of LEF versus CEF. The particular features of the CEF operating in maize (Ivanov et al., 2007; Laisk et al., 2010; Munekage et al., 2010; Hertle et al., 2013) may reflect, beyond the heterogeneity between BS and M specialization, this characteristic need for plasticity in CEF/LEF engagement.

Regardless of this electron transport plasticity, the ATP production deficits induced by changing light quality cannot be rebalanced within the individual BS chloroplast. In fact, increasing ATP production at the electron transport chain level would require light (Takabayashi et al., 2005; Kramer and Evans, 2011), whose availability is not under metabolic control. At the same time, the electron transport-mediated dark production of ATP (Morstadt et al., 2002; Bukhov and Carpentier, 2004; Egorova and Bukhov, 2004; Kuntz, 2004) has low conversion efficiency (Kramer and Evans,

2011); hence, an engagement of ATP chemiosynthesis would be incompatible with the observed pattern of J_{ATP}/GA. ATP itself is not a suitable shuttle to rebalance ATP deficits because the ATP molecule is relatively big, it has a relatively small pool, and homeostasis is critical; therefore, every chloroplast has an independent ATP pool. Maintaining balanced ATP consumption in spite of local ATP deficits therefore requires rearranging the localization of ATP demand, the fluxes, and the partitioning of metabolic work between the mutually interdependent BS and M cells.

Metabolic Plasticity Is Effective in Maintaining Overall Assimilation Efficiency

Previously, on the basis of theoretical considerations, it had been predicted that an unbalanced ATP supply would result in a disruption of the delicate equilibrium between BS and M functions with consequent loss in assimilatory efficiency (Henderson et al., 1992; Evans et al., 2007; Tazoe et al., 2008). This prediction arose because metabolic rigidity would be expected under some of the common simplifications used for C_4 biochemistry, whereby transamination is neglected, PGA is reduced at a fixed rate in BS, and NADPH delivery to BS is equimolar to CO_2 delivery (Laisk and Edwards, 2000, 2009). In the updated description of C_4 metabolism provided in this paper, reaction rates are variable and tunable. When the ATP availability in BS was low (e.g. condition 1), PR in BS was down-regulated, leaving all available ATP for RuBP regeneration, resulting in unaltered Rubisco efficiency. Because the Asp-mediated CCM delivers solely CO_2 while the MAL-mediated CCM delivers both NADPH and CO_2, the variable engagement of the two pathways allows the activity of the CCM to be regulated independently of NADPH demand in BS; hence, the optimal C_{BS} could be maintained under all light qualities.

These predictions are supported by further model outputs, where we found no significant effect of light quality on Φ and on C_{BS}, confirming the response found in a similar experiment where plants were acclimated under high light (Sun et al., 2012). This observation, together with the relatively minor change in J_{ATP}/GA (Fig. 4B), show that C_4 metabolic balance was adjusting to the shifts in ATP supply without the potential major disruptions mentioned above.

Implications for Light Use at the Leaf and Canopy Levels

Photosynthesis in shaded conditions has critical importance in C_4 canopies, as it may represent up to 50% of CO_2 uptake (Baker and Long, 1988; Long, 1993). Shade light has a reduced intensity (typically one-twentieth of full sunlight; Shirley, 1929) and differs in spectral quality from red-rich sunlight: diffuse sky radiation is enriched in blue, whereas canopy-filtered light is enriched in green (Smith, 1982). Under low-light conditions, it has been shown that Φ may increase both at the leaf

(Kromdijk et al., 2010; Bellasio and Griffiths, 2013) and canopy (Kromdijk et al., 2008) levels. Theoretical considerations have associated this Φ increase with decreased C$_4$ efficiency and a potential loss of photosynthetic carbon uptake (Furbank et al., 1990; von Caemmerer, 2000; Kromdijk et al., 2008; Tazoe et al., 2008). Although other studies have compared the effect of light quality on Φ under low irradiance or under different light qualities (Kromdijk et al., 2010; Sun et al., 2012; Bellasio and Griffiths, 2013; Ubierna et al., 2013), the novelty of the approach presented here has been to couple the measured and predicted ATP supply during assimilation under these conditions. In this experiment, which was specifically optimized to acquire data under low light (Bellasio and Griffiths, 2013), we showed that the total ATP cost of gross assimilation was not significantly influenced by light intensity and underwent a little variation under different light quality (Fig. 4B). This showed that metabolism at steady state under low light intensities maintained efficiency in spite of changes in light quality or intensity. This implies that the hyperbolic increase of Φ observed under decreasing light intensities (Fig. 3D), which underpins the predicted photosynthetic efficiency loss, actually did not cost additional ATP but resulted instead from mitochondrial decarboxylation in BS (Bellasio and Griffiths, 2013). Similar conclusions were highlighted by Ubierna et al. (2013). This observation is consistent with V_P/V_C (for Rubisco carboxylation rate) and the optimal x being largely independent of light intensity (von Caemmerer, 2000; Kromdijk et al., 2010), indicating a constant degree of engagement of the CCM even under an apparent Φ increase. Therefore, care should be taken when the ATP cost (and quantum yield) of C$_4$ photosynthesis is derived from Φ, measured either at the leaf or canopy scale, particularly in the vicinity of the light compensation point (Furbank et al., 1990; von Caemmerer, 2000; Tazoe et al., 2008). In these conditions, we propose that the ATP cost should be calculated by summing the ATP cost of all the active biochemical processes (see Eq. 11 in Table II) instead of using Φ as a proxy for C$_4$ biochemical efficiency. The actual impact of Φ on canopy-level carbon uptake may depend upon the extent of steady-state photosynthesis under low light or altered light quality conditions (e.g. green enriched), and shorter term, more transient conditions, when Φ may be more variable.

CONCLUSION

In this study, we set out to investigate whether the maize C$_4$ system could respond to changing environmental conditions by adjusting the C$_4$ (amino) acid (MAL or Asp) delivered from M to BS as well as the proportions of other metabolic reactions shared between both cell types, such as SS, PR, and PEP regeneration (Walker et al., 1986; Spilatro and Preiss, 1987; Wingler et al., 1999; Friso et al., 2010; Majeran et al., 2010; Furbank, 2011). Using contrasting light qualities and their projected extinctions within the leaf profile, we could then

estimate the rate of ATP synthesis in M and BS compartments as compared with the overall leaf-level operating efficiency measured by gas exchange and real-time carbon isotope discrimination. We depicted a scenario whereby metabolism, although subject to the general constraints imposed by C$_4$ physiology, was able to take maximum advantage of environmental conditions by changing the relative engagement of BS and M functions, which were ultimately under environmental control. The outputs, based on metabolic modeling and empirical measurements, provide definitive evidence for the role of complementarity between BS and M functions, allowing ATP demand to be regulated in response to contrasting environmental conditions. The two decarboxylase systems in BS of maize, with a variable rate of transamination, allow the regulation of NADPH supply to match demand in BS independently of the delivery of CO$_2$.

The findings of this study highlight the importance of C$_4$ metabolic models in helping to explain acclimation and adaptation to changing light intensity for all C$_4$ subgroups. The emerging complexity of the NADP-ME/PEPCK interactions certainly demands some refinement to the widespread simplifications used to describe C$_4$ systems and to the assumptions regarding the relatively fixed energetic partitioning in maize. Furthermore, we have clearly linked metabolic plasticity to the capacity to maintain high photosynthetic efficiency under changing environmental conditions, which could well be related to the original functions of BS decarboxylases and the evolution of the C$_4$ syndrome (Hibberd and Quick, 2002; Griffiths et al., 2013). Finally, the extent to which such steady-state conditions of low light and altered light quality affect carbon uptake within an intact crop canopy remains to be determined, as compared with more transient responses, which may well increase Φ and reduce carbon assimilation under low-light conditions.

MATERIALS AND METHODS

Metabolic Model

The processes contributing to assimilatory metabolism in maize (*Zea mays*; Furbank, 2011) were integrated in a comprehensive steady-state model (Fig. 1). Some functional simplifications were made. Cells were decompartmentalized. NADPH and NADH were considered equivalent or convertible. Starch was assumed to be the only final product of photosynthesis (SS has the same ATP cost per hexose than phloem-loaded Suc, considering the stoichiometry of one ATP per H$^+$ of the membrane H$^+$-ATPase and one H$^+$ per Suc of the Suc symporter). The ATP and NADH produced during respiration (assumed to be supplied by PGA) were neglected in calculations because they are likely to be consumed by basal metabolism. Transamination was assumed to be passively regulated by substrate availability (all OAA not reduced by MDH was transaminated), as transamination reactions are rapid conversions at equilibrium (see "Discussion").

The specialization of BS and M was captured by assigning processes to BS, M, or the conjoint work of both compartments (allocatable processes). PEPCK (Walker et al., 1986; Furumoto et al., 1999, 2000; Wingler et al., 1999) and glyoxylate recycling (Yoshimura et al., 2004) were allocated to BS; LEF (Meierhoff and Westhoff, 1993; Romanowska et al., 2006; Majeran and van Wijk, 2009; Friso et al., 2010; Kramer and Evans, 2011) and PPDK (see "Discussion") were allocated to M; R_{LIGHT} was split equally between M and BS (von Caemmerer, 2000; Kromdijk et al., 2010; Ubierna et al., 2011); PR and SS were variably allocated. T was equal in BS and M, as the pool of Asp and Ala is shared. The model was described by steady-state rate equations (Table II).

Minimum and Maximum BS Allocation

The rate of variably allocated processes ranged between a minimum rate and a maximum rate, deduced from physiological considerations (for the environmental influence on maximum rates, see "Discussion"). Both BS and M express SS enzymes (Spilatro and Preiss, 1987; Majeran and van Wijk, 2009) and synthesize starch (Rascio et al., 1980; Kanai and Edwards, 1999), so SS was allocated to BS between zero and total SS rate. PR is not essential to BS, so minimum PR was set at zero. PR is mainly an M process (Majeran et al., 2005; Majeran and van Wijk, 2009), so maximum PR rate in BS was limited at $0.35 \times$ total PR rate. PEPCK is not essential to BS, so minimum PEPCK was set at zero. Maximum PEPCK was set at $0.3 \times V_P$, identified by fitting the total ATP demand of assimilation to J_{ATP}/GA (Fig. 4B).

Parameterization

Equations describing overall assimilation (Eqs. 4–10 in Table II) were parameterized with the measured data A, R_{LIGHT}, the output of the von Caemmerer C_4 model (Rubisco oxygenation rate [V_O], V_P, and V_C; Supplemental Table S1; Bellasio and Griffiths, 2013), and Φ calculated from Δ under photosynthetically active radiation (PAR) = 125 μE m^{-2} s^{-1} (see below). Then, reaction rates (Eqs. 4–21 in Table II) were calculated under the minimum (condition 1) and the maximum (condition 3) BS allocation (Figs. 1 and 4B). Finally, intermediate states (e.g. condition 2) were calculated by allocating reactions to BS in linear increments (see continuous lines in Fig. 4A).

The ATP demand in BS was calculated by adding the ATP demand of BS processes (Eq. 12 in Table II; Supplemental Table S2). Analogously, ATP demand in M was calculated by summing the ATP demand of M processes (Eq. 13 in Table II; Supplemental Table S2), and ATP_{BS}/ATP_M was calculated by dividing Equation 12 by Equation 13. Similarly, $NADPH_{BS}$ was calculated by summing the NADPH demand of BS processes (Eq. 14 in Table II; Supplemental Table S2). Rate equations for other processes are listed in Table II.

Estimated AB BS/M

A maize leaf cross section was simulated by rectangular units, enclosing a square BS (Fig. 2, left). Interveinal distance (106 μm), M thickness (100 μm), BS/M area (0.26), and the resulting BS side (46 μm) were averaged from the literature (Hattersley, 1984; Usuda, 1985; Bongard-Pierce et al., 1996; Moreno-Sotomayor et al., 2002; Kromdijk et al., 2010). Because of the square anatomy, the leaf light environment could be described by two light profiles: P1 and P2. These were calculated applying the Kubelka-Munk absorption-scattering theory with the method of Allen and Richardson (1968) and others (Gates, 1980; Terashima et al., 2009), modified to describe the simulated C_4 anatomy. Briefly, each profile was considered to be made of a number n of light-absorbing and light-scattering elements; the total number of elements in the profile was N. The element $n = 0$ was the illuminated, or adaxial, point of the profile, which included the upper epidermis, approximated to a single reflecting element. The element N was the abaxial point of the profile, which included the lower epidermis, approximated to a single reflecting element. Radiant flux directed downward was I, and that upward was J. Incident flux was I_0 and was taken to be the unity. For each profile, the flux reflected by the first element was equivalent to the point reflectance and the flux transmitted by the last element was equivalent to the point transmittance: $J(0) = $ point reflectance and $I(N) = $ point transmittance.

Incremental absorption and scattering were calculated as (Gates, 1980):

$$(1)$$

$$(2)$$

where k is an absorption coefficient and s is a scattering coefficient. In P1, k was constant throughout the profile. In P2, k was three times higher in the elements corresponding to BS, because chlorophyll concentration is three times higher than in the surrounding M (BS/M chlorophyll content = 0.74 [Kanai and Edwards, 1973] multiplied by M/BS area = 4 [Fig. 2, left]). I and J were solved for all elements of P1 and P2 according to the integration of Equations 1 and 2 proposed by Gates (1980). Modeled leaf reflectance resulted from averaging $J(0)$ contributions to the total leaf reflectance from P1 and P2 (56% P1 and 44% P2). Similarly, modeled leaf transmittance was calculated as a weighted average of $I(N)$ from P1 and P2. Modeled leaf reflectance and transmittance were calibrated with measured leaf reflectance and transmittance at different wavelengths (Table III; Woolley, 1971) by varying k and s. This procedure allowed calculating P1 and P2 at different wavelengths (Fig. 2, right). AB in BS resulted from integrating P2 over BS area. AB in M resulted from integrating P2 over adaxial and abaxial M area (MAD + MAB) plus the integral of P1 over the two interveinal M areas (MI).

Estimated J_{ATPBS}/J_{ATPM}

M chloroplasts are engaged in NADPH and ATP production while BS chloroplasts only produce ATP; therefore, for a given number of light quanta, M chloroplasts produce approximately half the ATP produced in BS chloroplast. J_{ATPBS}/J_{ATPM} was calculated as:

$$(3)$$

The coefficient 2 (in Eq. 3) is based on a widely accepted assumption that light is equally shared between photosystems and on the simplification that the photochemical yield is independent of the position within the leaf profile. In detail, we assumed (1) exclusive linear electron transport in M with equal PSI/PSII absorption partitioning (Meierhoff and Westhoff, 1993; Kramer and Evans, 2011); (2) exclusive cyclic electron transport in BS with no PSII absorption (Romanowska et al., 2006; Majeran and van Wijk, 2009); (3) equal yield of PSI and PSII (Miyake et al., 2005; Supplemental Fig. S3C); (4) equal H$^+$/ATP stoichiometry of the ATP synthase in BS and M (the enzyme complex is the same; Majeran and van Wijk, 2009; Friso et al., 2010); and (5) twice the H$^+$ per photochemical event pumped in BS versus M: in M, 1.5 H$^+$ are extruded per photochemical event (Kramer and Evans, 2011), while in BS, we assumed three H$^+$ extruded per photochemical event (average between four H$^+$ of the NDH-mediated electron flow [Kramer and Evans, 2011; Peng et al., 2011] and two H$^+$ of the PGR5/PGRL1-mediated electron flow [Kramer and Evans, 2011; Hertle et al., 2013], both operating in maize BS [Ivanov et al., 2007]).

Plants

Maize (F1 hybrid PR31N27; Pioneer Hi-Bred) plants were grown in 1.5-L pots filled with Levington pro M3 (Scotts) in growth rooms (Conviron) set at 16-h daylength, temperature of 25°C/23°C (day/night), 40% relative humidity, and PAR = 600 μE m^{-2} s^{-1} and manually watered daily with particular care to avoid overwatering. After 3 weeks, plants were measured once and then discarded.

Gas-Exchange Measurements with Concurrent PSI/PSII Yield and Online Carbon Δ

The experimental setup was described previously (Bellasio and Griffiths, 2013). Briefly, an infrared gas analyzer (IRGA; LI6400XT; Li-Cor), was fitted with a 6400-06 PAM2000 adapter and with a Li-Cor 6400-18 RGB light source. The IRGA was fed with CO_2 ($\delta^{13}C = -8.3$‰; Isi Soda) and either a mixture of 2% oxygen/nitrogen or ambient air. PSI yield and PSII yield [$Y(II)$] were measured with a Dual Pam-F (Heinz Walz). The IRGA was connected to a cryogenic water- and CO_2-trapping purification line. To determine the relationship between $Y(II)$ and J_{ATP}, a light-response curve was measured at 2% oxygen and C_a = 600 μmol mol^{-1}. Under the same light quality, 21% oxygen, and reference CO_2 set at 400 μmol mol^{-1}, a second light-response curve was measured, during which $Y(II)$ was determined and exhaust gas was trapped to determine Δ. In 1 d, a total of 12 CO_2 samples and six CO_2 references from each individual plant were analyzed directly with a VG SIRA dual-inlet isotope ratio mass spectrometer (modified and maintained by Pro-Vac Services). Δ was calculated as reported in Supplemental Figure S2, using Equation 22. R_{LIGHT} was calculated as the y intercept of the linear regression of A against PAR $\times Y(II)/3$. J_{ATP} was calculated from chlorophyll fluorescence data, by calibrating the relationship between ETR and $Y(II)$ under low oxygen, and then using such a calibration to determine the small fraction of ATP consumed by photorespiration. The correction was minimal because of the low oxygen sensitivity of maize (Supplemental Table S1; Bellasio and Griffiths, 2013); therefore, the potential errors caused by using fluorescence measurements under contrasting light qualities were negligible. Light responses were treated with dedicated software (Photosyn assistant 1.2; Dundee Scientific) to calculate the light compensation point and by repeated-measures ANOVA (Genstat); point estimates were subject to ANOVA and Tukey's multiple comparison (Genstat).

Φ from Δ

Φ was resolved from Δ by use of the full Farquhar model (Farquhar, 1983; Farquhar and Cernusak, 2012), parameterized with a C_4 photosynthesis model (von Caemmerer, 2000), using equations and a fitting approach that were

described previously (Supplemental Table S1; Bellasio and Griffiths, 2013). Briefly, Φ was resolved from Δ by calculating the weighted individual fractionations of the discriminating processes operating in C$_4$ photosynthesis. The CO$_2$ concentration in the cellular compartments was calculated by means of a C$_4$ model, parameterized with the light-response data (A, Ci, Ca, and J_{ATP}) and R_{LIGHT}. The C$_4$ model was rearranged to express a modeled ATP production rate J_{MOD} and fit to the J_{ATP} (Supplemental Table S1), to yield a value for BS conductance for each individual plant, independently from Δ.

Supplemental Data

The following materials are available in the online version of this article.

Supplemental Figure S1. Ecophysiological responses to decreasing light intensity under different light qualities.

Supplemental Figure S2. ξ values for the calculation of Δ.

Supplemental Figure S3. Photochemical responses to decreasing light intensity under different light qualities.

Supplemental Table S1. Definitions, equations, and variables used in the models.

Supplemental Table S2. ATP and NADPH demand for key C$_4$ processes.

LITERATURE CITED

Allen WA, Richardson AJ (1968) Interaction of light with a plant canopy. J Opt Soc Am **58:** 1023–1028

Aoyagi K, Nakamoto H (1985) Pyruvate, Pi dikinase in bundle sheath strands as well as in mesophyll cells in maize leaves. Plant Physiol **78:** 661–664

Baker NR, Long SP (1988) Photosynthesis and temperature, with particular reference to effects on quantum yield. *In* SP Long, FI Woodward, eds, Plants and Temperature: Society for Experimental Biology Symposium No XXXXII. Company of Biologists, London, pp 347–375

Bellasio C, Griffiths H (October 8, 2013) Acclimation to low light by C4 maize: implications for bundle sheath leakiness. Plant Cell Environ http://dx.doi.org/10.1111/pce.12194

Berry JA, Farquhar GD (1978) The CO$_2$ concentrating function of C4 photosynthesis: a biochemical model. *In* D Hall, J Coombs, T Goodwin, eds, Proceedings of the 4th International Congress on Photosynthesis. Biochemical Society, London, pp 119–131

Bongard-Pierce DK, Evans MMS, Poethig RS (1996) Heteroblastic features of leaf anatomy in maize and their genetic regulation. Int J Plant Sci **157:** 331–340

Bukhov N, Carpentier R (2004) Alternative photosystem I-driven electron transport routes: mechanisms and functions. Photosynth Res **82:** 17–33

Chapman KSR, Hatch MD (1981) Aspartate decarboxylation in bundle sheath cells of Zea mays and its possible contribution to C-4 photosynthesis. Aust J Plant Physiol **8:** 237–248

Covshoff S, Hibberd JM (2012) Integrating C4 photosynthesis into C3 crops to increase yield potential. Curr Opin Biotechnol **23:** 209–214

Detarsio E, Wheeler MCG, Campos Bermúdez VA, Andreo CS, Drincovich MF (2003) Maize C4 NADP-malic enzyme: expression in Escherichia coli and characterization of site-directed mutants at the putative nucleoside-binding sites. J Biol Chem **278:** 13757–13764

Downton WJS (1970) Preferential C4-dicarboxylic acid synthesis, the postillumination CO$_2$ burst, carboxyl transfer step, and grana configurations in plants with C4-photosynthesis. Can J Bot **48:** 1795–1800

Drincovich MF, Andreo CS (1994) Redox regulation of maize NADP-malic enzyme by thiol-disulfide interchange: effect of reduced thioredoxin on activity. Biochim Biophys Acta **1206:** 10–16

Egorova EA, Bukhov NG (2004) Modeling of alternative pathways of electron transport to photosystem I in isolated thylakoids. Russ J Plant Physiol **51:** 579–583

Eprintsev AT, Fedorina OS, Bessmeltseva YS (2011) Response of the malate dehydrogenase system of maize mesophyll and bundle sheath to salt stress. Russ J Plant Physiol **58:** 448–453

Evans JR, Sharkey TD, Berry JA, Farquhar GD (1986) Carbon isotope discrimination measured concurrently with gas-exchange to investigate CO$_2$ diffusion in leaves of higher-plants. Aust J Plant Physiol **13:** 281–292

Evans JR, von Caemmerer S, Vogelmann TC (2007) Balancing light capture with distributed metabolic demand during C4 photosynthesis. *In* JE Sheehy, PL Mitchell, B Hardy, eds, Charting New Pathways to C4 Rice. International Rice Research Institute, Los Baños, Philippines, pp 127–143

Farquhar GD (1983) On the nature of carbon isotope discrimination in C4 species. Aust J Plant Physiol **10:** 205–226

Farquhar GD, Cernusak LA (2012) Ternary effects on the gas exchange of isotopologues of carbon dioxide. Plant Cell Environ **35:** 1221–1231

Friso G, Majeran W, Huang MS, Sun Q, van Wijk KJ (2010) Reconstruction of metabolic pathways, protein expression, and homeostasis machineries across maize bundle sheath and mesophyll chloroplasts: large-scale quantitative proteomics using the first maize genome assembly. Plant Physiol **152:** 1219–1250

Furbank R, Jenkins C, Hatch M (1990) C4 photosynthesis: quantum requirement, C4 and overcycling and Q-cycle involvement. Funct Plant Biol **17:** 1–7

Furbank RT (2011) Evolution of the C(4) photosynthetic mechanism: are there really three C(4) acid decarboxylation types? J Exp Bot **62:** 3103–3108

Furumoto T, Hata S, Izui K (1999) cDNA cloning and characterization of maize phosphoenolpyruvate carboxykinase, a bundle sheath cell-specific enzyme. Plant Mol Biol **41:** 301–311

Furumoto T, Hata S, Izui K (2000) Isolation and characterization of cDNAs for differentially accumulated transcripts between mesophyll cells and bundle sheath strands of maize leaves. Plant Cell Physiol **41:** 1200–1209

Gates DM (1980) Biophysical Ecology. Springer Verlag, New York

Griffiths H, Weller G, Toy LFM, Dennis RJ (2013) You're so vein: bundle sheath physiology, phylogeny and evolution in C3 and C4 plants. Plant Cell Environ **36:** 249–261

Hatch MD (1971) The C4-pathway of photosynthesis: evidence for an intermediate pool of carbon dioxide and the identity of the donor C4-dicarboxylic acid. Biochem J **125:** 425–432

Hattersley PW (1984) Characterization of C-4 type leaf anatomy in grasses (Poaceae), mesophyll-bundle sheath area ratios. Ann Bot (Lond) **53:** 163–179

Henderson SA, Von Caemmerer S, Farquhar GD (1992) Short-term measurements of carbon isotope discrimination in several C4 species. Aust J Plant Physiol **19:** 263–285

Hertle AP, Blunder T, Wunder T, Pesaresi P, Pribil M, Armbruster U, Leister D (2013) PGRL1 is the elusive ferredoxin-plastoquinone reductase in photosynthetic cyclic electron flow. Mol Cell **49:** 511–523

Hibberd JM, Quick WP (2002) Characteristics of C4 photosynthesis in stems and petioles of C3 flowering plants. Nature **415:** 451–454

Ivanov B, Asada K, Edwards GE (2007) Analysis of donors of electrons to photosystem I and cyclic electron flow by redox kinetics of P700 in chloroplasts of isolated bundle sheath strands of maize. Photosynth Res **92:** 65–74

Ivanov B, Asada K, Kramer DM, Edwards G (2005) Characterization of photosynthetic electron transport in bundle sheath cells of maize. I. Ascorbate effectively stimulates cyclic electron flow around PSI. Planta **220:** 572–581

Ivanov BN, Sacksteder CA, Kramer DM, Edwards GE (2001) Light-induced ascorbate-dependent electron transport and membrane energization in chloroplasts of bundle sheath cells of the C4 plant maize. Arch Biochem Biophys **385:** 145–153

Johnson HS, Hatch MD (1970) Properties and regulation of leaf nicotinamide-adenine dinucleotide phosphate-malate dehydrogenase and 'malic' enzyme in plants with the C4-dicarboxylic acid pathway of photosynthesis. Biochem J **119:** 273–280

Kanai R, Edwards GE (1973) Separation of mesophyll protoplasts and bundle sheath cells from maize leaves for photosynthetic studies. Plant Physiol **51:** 1133–1137

Kanai R, Edwards GE (1999) The biochemistry of C4 photosynthesis. *In* RF Sage, RK Monson, eds, C4 Plant Biology. Academic Press, San Diego, pp 49–87

Kramer DM, Evans JR (2011) The importance of energy balance in improving photosynthetic productivity. Plant Physiol **155:** 70–78

Kromdijk J, Griffiths H, Schepers HE (2010) Can the progressive increase of C_4 bundle sheath leakiness at low PFD be explained by incomplete suppression of photorespiration? Plant Cell Environ **33:** 1935–1948

Kromdijk J, Schepers HE, Albanito F, Fitton N, Carroll F, Jones MB, Finnan J, Lanigan GJ, Griffiths H (2008) Bundle sheath leakiness and light limitation during C4 leaf and canopy CO_2 uptake. Plant Physiol **148:** 2144–2155

Kuntz M (2004) Plastid terminal oxidase and its biological significance. Planta **218:** 896–899

Laisk A, Edwards G (2009) Leaf C4 photosynthesis in silico: the CO2 concentrating mechanism. Advances in Photosynthesis and Respiration **29:** 323–348

Laisk A, Edwards GE (2000) A mathematical model of C(4) photosynthesis: the mechanism of concentrating CO(2) in NADP-malic enzyme type species. Photosynth Res **66:** 199–224

Laisk A, Talts E, Oja V, Eichelmann H, Peterson RB (2010) Fast cyclic electron transport around photosystem I in leaves under far-red light: a proton-uncoupled pathway? Photosynth Res **103:** 79–95

Long SP (1993) The significance of light-limited photosynthesis to crop canopy carbon gain and productivity: a theoretical analysis. *In* YP Abrol, P Mohanty, Govindjee, eds, Photosynthesis: Photoreactions to Plant Productivity. Oxford & IBH Publishing, New Delhi, India, pp 547–560

Majeran W, Cai Y, Sun Q, van Wijk KJ (2005) Functional differentiation of bundle sheath and mesophyll maize chloroplasts determined by comparative proteomics. Plant Cell **17:** 3111–3140

Majeran W, Friso G, Ponnala L, Connolly B, Huang MS, Reidel E, Zhang CK, Asakura Y, Bhuiyan NH, Sun Q, et al (2010) Structural and metabolic transitions of C4 leaf development and differentiation defined by microscopy and quantitative proteomics in maize. Plant Cell **22:** 3509–3542

Majeran W, van Wijk KJ (2009) Cell-type-specific differentiation of chloroplasts in C4 plants. Trends Plant Sci **14:** 100–109

Meierhoff K, Westhoff P (1993) Differential biogenesis of photosystem-II in mesophyll and bundle-sheath cells of monocotyledonous NADP-malic enzyme-type C-4 plants: the nonstoichiometric abundance of the subunits of photosystem-II in the bundle-sheath chloroplasts and the translational activity of the plastome-encoded genes. Planta **191:** 23–33

Meister M, Agostino A, Hatch MD (1996) The roles of malate and aspartate in C-4 photosynthetic metabolism of Flaveria bidentis (L). Planta **199:** 262–269

Miyake C, Miyata M, Shinzaki Y, Tomizawa K (2005) CO2 response of cyclic electron flow around PSI (CEF-PSI) in tobacco leaves: relative electron fluxes through PSI and PSII determine the magnitude of non-photochemical quenching (NPQ) of Chl fluorescence. Plant Cell Physiol **46:** 629–637

Moreno-Sotomayor A, Weiss A, Paparozzi ET, Arkebauer TJ (2002) Stability of leaf anatomy and light response curves of field grown maize as a function of age and nitrogen status. J Plant Physiol **159:** 819–826

Morstadt L, Gräber P, De Pascalis L, Kleinig H, Speth V, Beyer P (2002) Chemiosmotic ATP synthesis in photosynthetically inactive chromoplasts from Narcissus pseudonarcissus L. linked to a redox pathway potentially also involved in carotene desaturation. Planta **215:** 134–140

Munekage YN, Eymery F, Rumeau D, Cuiné S, Oguri M, Nakamura N, Yokota A, Genty B, Peltier G (2010) Elevated expression of PGR5 and NDH-H in bundle sheath chloroplasts in C4 Flaveria species. Plant Cell Physiol **51:** 664–668

Murmu J, Chinthapalli B, Raghavendra AS (2003) Light activation of NADP malic enzyme in leaves of maize: marginal increase in activity, but marked change in regulatory properties of enzyme. J Plant Physiol **160:** 51–56

Peng L, Yamamoto H, Shikanai T (2011) Structure and biogenesis of the chloroplast NAD(P)H dehydrogenase complex. Biochim Biophys Acta **1807:** 945–953

Pick TR, Bräutigam A, Schlüter U, Denton AK, Colmsee C, Scholz U, Fahnenstich H, Pieruschka R, Rascher U, Sonnewald U, et al (2011) Systems analysis of a maize leaf developmental gradient redefines the current C4 model and provides candidates for regulation. Plant Cell **23:** 4208–4220

Rascio N, Colombo PM, Orsenigo M (1980) The ultrastructural development of plastids in leaves of maize plants exposed to continuous illumination. Protoplasma **102:** 131–139

Rathnam CKM (1978) Studies with isolated bundle sheath mitochondria: evidence for NAD-malic enzyme-catalyzed decarboxylation of C4 acids in species representing 3 C4 metabolic subtypes. FEBS Lett **96:** 367–372

Romanowska E, Drozak A, Pokorska B, Shiell BJ, Michalski WP (2006) Organization and activity of photosystems in the mesophyll and bundle sheath chloroplasts of maize. J Plant Physiol **163:** 607–618

Sage RF, Sage TL, Kocacinar F (2012) Photorespiration and the evolution of C4 photosynthesis. Annu Rev Plant Biol **63:** 19–47

Schulze S, Mallmann J, Burscheidt J, Koczor M, Streubel M, Bauwe H, Gowik U, Westhoff P (2013) Evolution of C4 photosynthesis in the genus *Flaveria*: establishment of a photorespiratory CO_2 pump. Plant Cell **25:** 2522–2535

Shirley HL (1929) The influence of light intensity and light quality upon the growth of plants. Am J Bot **16:** 354–390

Smith H (1982) Light quality, photoperception, and plant strategy. Annu Rev Plant Physiol **33:** 481–518

Spilatro SR, Preiss J (1987) Regulation of starch synthesis in the bundle sheath and mesophyll of *Zea mays* L.: intercellular compartmentalization of enzymes of starch metabolism and the properties of the ADPglucose pyrophosphorylases. Plant Physiol **83:** 621–627

Takabayashi A, Kishine M, Asada K, Endo T, Sato F (2005) Differential use of two cyclic electron flows around photosystem I for driving CO2-concentration mechanism in C4 photosynthesis. Proc Natl Acad Sci USA **102:** 16898–16903

Tazoe Y, Hanba YT, Furumoto T, Noguchi K, Terashima I (2008) Relationships between quantum yield for CO2 assimilation, activity of key enzymes and CO2 leakiness in Amaranthus cruentus, a C4 dicot, grown in high or low light. Plant Cell Physiol **49:** 19–29

Terashima I, Fujita T, Inoue T, Chow WS, Oguchi R (2009) Green light drives leaf photosynthesis more efficiently than red light in strong white light: revisiting the enigmatic question of why leaves are green. Plant Cell Physiol **50:** 684–697

Trost P, Fermani S, Marri L, Zaffagnini M, Falini G, Scagliarini S, Pupillo P, Sparla F (2006) Thioredoxin-dependent regulation of photosynthetic glyceraldehyde-3-phosphate dehydrogenase: autonomous vs. CP12-dependent mechanisms. Photosynth Res **89:** 263–275

Ubierna N, Sun W, Cousins AB (2011) The efficiency of C(4) photosynthesis under low light conditions: assumptions and calculations with CO (2) isotope discrimination. J Exp Bot **62:** 3119–3134

Ubierna N, Sun W, Kramer DM, Cousins AB (2013) The efficiency of C4 photosynthesis under low light conditions in Zea mays, Miscanthus × giganteus and Flaveria bidentis. Plant Cell Environ **36:** 365–381

Usuda H (1985) Changes in levels of intermediates of the C4 cycle and reductive pentose phosphate pathway during induction of photosynthesis in maize leaves. Plant Physiol **78:** 859–864

von Caemmerer S (2000) Biochemical Models of Leaf Photosynthesis. CSIRO, Canberra, Australia

Walker GH, Izawa S (1979) Photosynthetic electron transport in isolated maize bundle sheath cells. Plant Physiol **63:** 133–138

Walker GH, Ku MSB, Edwards GE (1986) Activity of maize leaf phosphoenolpyruvate carboxylase in relation to tautomerization and non-enzymatic decarboxylation of oxaloacetate. Arch Biochem Biophys **248:** 489–501

Wingler A, Walker RP, Chen ZH, Leegood RC (1999) Phosphoenolpyruvate carboxykinase is involved in the decarboxylation of aspartate in the bundle sheath of maize. Plant Physiol **120:** 539–546

Woolley JT (1971) Reflectance and transmittance of light by leaves. Plant Physiol **47:** 656–662

Yin XY, Struik PC (2012) Mathematical review of the energy transduction stoichiometries of C(4) leaf photosynthesis under limiting light. Plant Cell Environ **35:** 1299–1312

Yoshimura Y, Kubota F, Ueno O (2004) Structural and biochemical bases of photorespiration in C4 plants: quantification of organelles and glycine decarboxylase. Planta **220:** 307–317

Zhu X-G, Long SP, Ort DR (2010) Improving photosynthetic efficiency for greater yield. Annu Rev Plant Biol **61:** 235–261